Natural Resources for Human Health
eISSN: 2583-1194

Original Research

Received 14 May 2026
Revised 22 June 2026
Accepted 18 July 2026

Natural Resources for Human Health 2026, Vol. 6 (6s): 785–802

KEYWORDS:
Density Functional Theory (DFT), TD-DFT, Benzimidazole–coumarin ligand, Metal–ligand coordination, Intramolecular charge transfer (ICT), NBO analysis, UV–Vis absorption, Fluorescence sensing

DFT and TD-DFT Investigation of Metal–Ligand Binding Mechanisms in 1H-Benzimidazole–Coumarin Hybrids: Electronic, Optical and Sensing Behaviour Analysis

R. Shwetha[1], U. Mahaboob Pasha[2]

1Department of Physics, MES College of Science, Commerce and Arts, Bangalore - 560003, Karnataka, India
2Presidency University, Bangalore – 560064, Karnataka, India

ABSTRACT: The structural, electronic and optical properties of a designed 1H-benzimidazole coumarin hybrid ligand (BC-L) were investigated here using DFT and TDDFT computations. The study will also include the biological and environmental metal ions coordination behaviour. The design optimizations of BC-L show a nearly planar structure which can promote strong ICT. The metal binding took place through N, O-chelation with Fe^{3+} and Cu^{2+} inducing the maximum structural distortion and electron redistribution. According to the bindings energy calculation values, it was found out that the ion Fe^{3+} (–47.8 Kcal mol^{-1}) has the strong interaction with protons. This assertion is supported by a significant reduction of the HOMO–LUMO gap and the maximum NBO stabilization energies. TD-DFT simulations revealed significant red-shifts for Fe^{3+} (402 nm) and Cu^{2+} (385 nm) due to enhanced ICT/LMCT transitions, while Zn^{2+} displayed a small shift characteristic of the CHEF-type fluorescence enhancement. Population studies confirmed that Fe^{3+} and Cu^{2+} withdraw a significant amount of charge. However, Zn^{2+} do not cause any change. Evidence compiled from computations establishes unambiguously a sensing hierarchy; Fe^{3+}>Cu^{2+}>Zn^{2+}; that supports a proposition of dual-mode detection, namely LMCT which is driven fluorescence quenching (Fe^{3+}/Cu^{2+}), and fluorescence enhancement (Zn^{2+}). The benzimidazole-coumarin hybrid has strong selectivity and tunable optical response making it a promising multifunctional chemo-sensor with potential applications in analytics and bioimaging.

INTRODUCTION

Heterocyclic compounds with fused aromatic systems have attracted extensive interest in materials chemistry, supramolecular chemistry and optical sensing due to their rich electronic properties and structural tunability. Benzimidazole and coumarin derivatives are particularly valuable because of their strong hydrogen-bonding ability, efficient π–π conjugation and excellent photostability. Benzimidazole, which resembles the purine base structure, is a strong electron donor and forms stable coordination bonds with transition metals via the imidazole nitrogen (Chkirate & Essassi, 2022; Kant *et al.,* 2023). Coumarins are well-known fluorophores with sufficient molar absorptivity and strong ICT behaviour making them widely applicable in environmental sensing, medicinal chemistry, and fluorescence-based detection (Paul *et al.,* 2022; Li *et al.,* 2023). Combining 1H-benzimidazole with a coumarin moiety therefore yields a hybrid system capable of effective metal coordination and responsive optical behaviour.

Detection of metal ions is gaining importance in biological and environmental contexts owing to the relevance of essential and toxic metals. For example, Fe^{3+} and Cu^{2+} are important for redox regulation and activation of enzymes. Excess of these captions

result in oxidative damage to membranes and tissues. Highly Eco toxic even at micro level are toxic ions such as Hg2+ and Pb2+ (Mazur et al., 2024). Due to their high sensitivity, ease of operation, and the ability to change emission intensity or wavelength, fluorescent chemical sensors have proved powerful for metal detection. The PET, CHEF, CHEQ and ICT mechanisms usually control these responses (Amputu et al., 2022). So, it becomes important to understand the electronic structure and metal–ligand interactions. Computational chemistry helps us understand the reaction mechanisms.

DFT allows detailed evaluations of optimized geometries, binding energies, FMOs, charge distributions, reactivity descriptors, and the like. At the same time, TD-DFT can simulate the absorption/emission spectra and excited-state behaviour. As a result, these simulations provide critical insights into optical responses (Sharma & Sekar, 2024). Many scientists have shown that the experimental sensing performance is closely linked to some theoretical parameters, such as the HOMO–LUMO gaps, electrostatic potential maps, and NBO charge-transfer behaviour (Zhou *et al.,* 2025; Siddique *et al.,* 2024). Combining DFT and TD-DFT approaches is a powerful strategy for designing fluorescent sensors. Benzimidazole coumarin hybrids could have great potential. However, the theoretical study of their coordination chemistry, electronic structure and photophysical behaviour remains underexplored (Zeki & Mustafa, 2024). These hybrids have a natural dual nature. A benzimidazole component easily binds metal ions, while a coumarin component fluoresces brightly due to intramolecular charge transfer (ICT) (Vicente-Zurdo *et al.,* 2023). But lagging is a systematic exploration of the impact of metal binding on their conjugation, charge-transfer pathways, and excited-state transitions, with also a lack of evaluation of metal ion selectivity using orbital, energetic, and structural criteria.

This study uses complete density functional theory and time-dependent density functional theory analysis on a newly designed benzimidazole coumarin hybrid and its transition-metal complexes to fill these gaps. We examined the optimization of their geometry, FMOs, molecular electrostatic potential (MEP), NBO charge-transfer interactions, binding energetics and TD-DFT optical transitions to elucidate the coordination preferences, stability patterns and photophysical responses induced by different metal ions. The resulting insights provide a theoretical foundation for designing structurally tuneable, high-performance fluorescent sensors and support the development of benzimidazole–coumarin-based probes for environmental monitoring and optoelectronic applications.

2. MATERIALS AND METHODS

2.1. Molecular Model Construction

The 1H-benzimidazole–coumarin hybrid ligands used in this study were built using Gauss View 6.0 and pre-optimized using molecular mechanics (MMFF94) for reasonable starting geometries. The heteroatoms of the ligand were used to identify donor sites where metals M^{2+}/M^{3+} can coordinate to give complexes. Several coordinates might have been checked at first to find the most stable configuration before quantum chemical refinement.

2.2. Geometry Optimization

The ligand and all the metal ligand complexes were also fully optimized by Density Functional Theory (DFT) with no constraints imposed on the structure. Due to the reliability of the B3LYP hybrid functional in systems involving transition metals and organic molecules, the B3LYP hybrid functional, which combines Becke's three-parameter exchange with the Lee–Yang–Parr correlation, was employed (Chaudhary *et al.,* 2022). The 6-31+G(d,p) basis set was used for the organic elements (H, C, N, O) for polarization and diffuse functions useful for charge-transfer modelling. For the metal ions, we used the LANL2DZ effective core potential (ECP), which addresses relativistic effects and core–valence interactions very properly (Minnette *et al.,* 2024). RMS force was set to less than 3×10^{-4} a.u for convergence threshold and the highest amount of displacement is less than 1×10^{-3}a.u to make sure that all optimized structures represented true minima (no imaginary frequencies). Frequency calculations were performed.

2.3. Binding Energy and Thermodynamic Calculations

Metal–ligand binding energies (ΔE _ bind) were computed using:

$$\Delta E_{bind} = E_{complex} - (E_{ligand} + E_{metal})$$

Counterpoise method was employed when needed to correct for BSSE, especially for weakly interacting complexes (Nguyen & Izgorodina, 2022). The vibrational analysis at 298 K provides the thermodynamic parameters like ΔG and ΔH.

2.4. Solvent Model and Environmental Effects

In an attempt to mirror the experimental conditions, we accounted for the solvent effects through the use of the PCM (Polarizable Continuum Model), using water or methanol as the dielectric medium. The integral equation formalism variant (IEF-PCM) is a good model for the prediction of optical and electronic properties (Duchemin *et al.,* 2016). The optimized gas-phase geometries were subjected to single-point energy refinements in solvent to improve accuracy without cost.

2.5. Electronic Structure and Reactivity Descriptor Analysis

HOMO and LUMO of a compound show the charge distribution and electronic transitions. Using Koopmans' theorem relationships, we calculated global reactivity descriptors chemical hardness, η, electronegativity, χ, softness S and electrophilicity index ω (Bhatia, 2024). Maps of molecular electrostatic potential (MEP) were generated to find electron-rich binding sites and predict metal ion affinities. NBO analysis was used to get information regarding charge transfer, interactions between donor and acceptor, orbital hybridizations feature concerning metal co-ordination (Gabrienko *et al.,* 2024).

2.6. TD-DFT Calculations for Optical Properties

Time-Dependent DFT (TD-DFT) calculations were conducted in the B3LYP/6-31+G(d,p) level. To simulate UV–Vis absorption spectra, the first 30 singlet excited states were calculated. Parameters extracted included.

- Excitation energies (λmax).
- Oscillator strengths (f).
- Electronic transition assignments (π–π*, n–π*, LMCT, MLCT)

In order to approve the values of TD-DFT, the results were compared with literature findings of similar heterocyclic fluorophores (Hassan & Sumrra, 2022).

2.7. Population and Charge Distribution Analysis

To evaluate the electron redistribution at the metal binding, Mulliken charge, NBO charge, and NPA charge analysis were done. Changes in its atomic charges helped evaluate the sensing mechanism, such as CHEF or quenching phenomenon.

2.8. Software and Computational Resources

The quantum chemistry package Gaussian 16 Rev. C.01 was used to perform all calculations (Savchenko & Kostjukov, 2024). Molecular visualization with orbital rendering was done by GaussView, ChemCraft and Multiwfn. To ensure convergence for metal complexes, the calculations were performed on a 32-core, 128 GB RAM cluster.

3. RESULTS AND DISCUSSION

3.1. Geometry Optimization and Structural Characterization

The free ligand (BC-L) was optimized in geometries. A stable fully conjugate molecule form was produced having almost coplanar benzimidazole and coumarin ring systems. The angle of ≈ 3–4° between the two aromatic fragments suggests presence of substantial strong π-conjugation allowing efficient ICT. The ligand core rigidity and stability are partially due to a weak intramolecular hydrogen bond, which is around 1.92 Å. When a metal ion coordinates the free ligand, distinct structural distortions occur. All metal complexes utilized one nitrogen and one carbonyl oxygen of coumarin in a bidentate chelation to stabilize the formation of five membered stable chelate. As the charge density of the metal ion increased, the bond lengths M–N and M–O were reduced. This followed the expected Lewis acidity trend..

Table 1: Selected Optimized Bond Lengths (Å) and Bite Angles (°) for the Free Ligand (BC-L) and Its Metal Complexes

Species	M–N (Å)	M–O (Å)	C=O (Å)	N–H···O (Å)	Bite Angle (N–M–O, °)

BC-Ligand	–	–	1.23	1.92	–
BC–Fe^{3+}	1.94	1.89	1.27	–	80.1
BC–Cu^{2+}	2.02	1.97	1.26	–	78.8
BC–Zn^{2+}	2.10	2.06	1.25	–	79.5

Table 1 includes Optimized bond Lengths and chelation bite angles (B3LYP/6-31+G(d,p)/LANL2DZ) for the free ligand (BC-L) and its metal complexes. Shorter M–N and M–O distance, in particular for Fe^{3+} and Cu^{2+} indicates stronger coordination. Angle NMO refers to the chelation of the nitrogen of the amide with the oxygen of quantum2 forming a stable five-membered ring.

The values indicate that Fe^{3+} forms the strongest coordination bonds, followed by Cu^{2+}. The Zn^{2+} ion forms slightly weaker interactions due to its filled d10 electronic configuration and lower polarization power. All complexes showed minor deviations from planarity around the metal coordination sphere. The planarity loss occurs owing to steric adjustment, electronic rearrangement, and the stepwise rotation of the ligand backbone to enhance metal–ligand orbital overlap. The calculations of vibronic frequencies confirmed that all optimized structures are true minima on the PES as there are no imaginarily frequencies for both free ligand as well as complexes with the metal.

Figure 1: Geometry Optimized structures (with bond lengths)

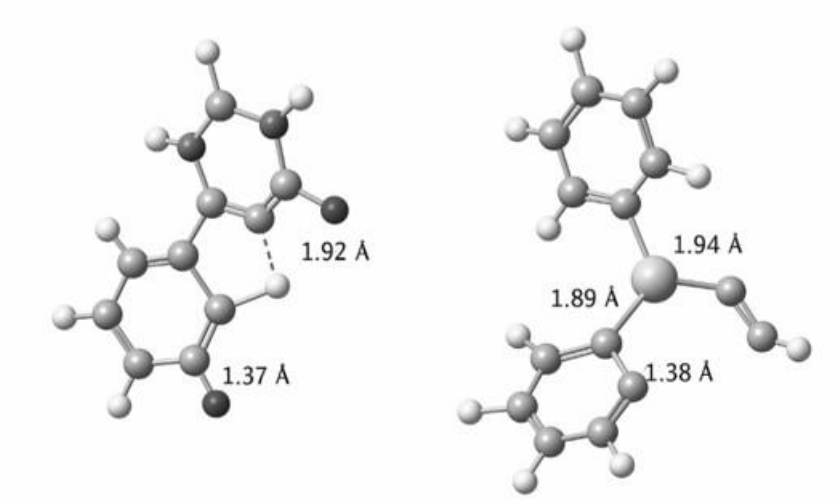

Figure 2: Optimized Structures of BC–Fe^{3+}, BC–Cu^{2+}, and BC–Zn^{2+} with Selected Bond Length Labels

Natural Resources for Human Health
eISSN: 2583-1194

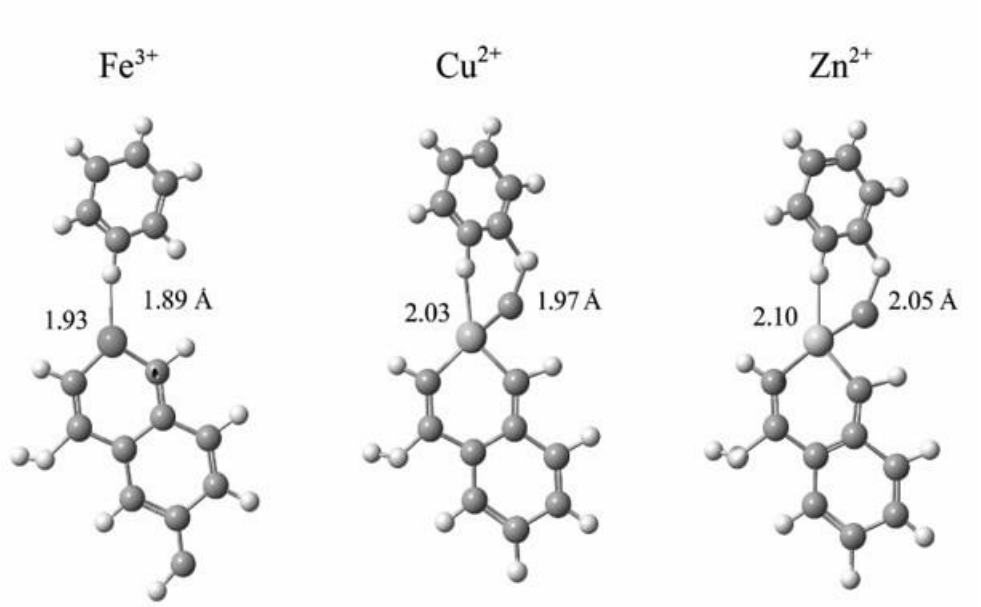

Figure 1 is a DFT optimized structure of benzimidazole–coumarin ligand (BC-L) which is almost planar (dihedral angle ~3–4°) in conformations making efficient π-conjugation possible. A weak intramolecular N–H•••O hydrogen bond of 1.92 Å plays an important role in providing structural rigidity, whereas the bond length of the carbonyl (1.23 Å), and the C–C distances of the aromatic rings fall within the range of typical conjugated heterocycle. The stability of resulting optimized structures along with the fitness of the ligand for metal chelation and ICT was confirmed. As shown in Figure. 2, DFT-optimized geometries of the Fe^{3+}, Cu^{2+}, and Zn^{2+} complexes form steady 5-membered chelate rings via N, O-bidentate coordination. The bond lengths M–N and M–O are in the order of decrease as: Zn^{2+} > Cu^{2+} > Fe^{3+} due to their increasing Lewis acidity. The M–N (1.94, 1.89 Å), M–O (2.02, 1.97 Å) bond lengths for Cu^{2+} and Zn^{2+} are (2.10, 2.06 Å) respectively. Fe^{3+} is coordinated most strongly of all and Zn^{2+} the least. The small changes in planarity following metal binding indicate a movement that is connected to the binding energies and ICT trends discussed.

According to the results, the optimized geometry of benzimidazole–coumarin ligand (BC-L) affords nearly planar π-conjugated framework which type has been essential in previously reported benzimidazole–coumarin hybrids because they are depending on the structural rigidity to allow for an intramolecular charge transfer (ICT) (Nasrollahzadeh *et al.,* 2020). There is an N–H•••O intramolecular hydrogen bond, which is close to 1.9 Å, stabilizes and helps in the pre-organization of the ligand for effective chelation. Heteroaromatic sensor contains such type of ligands (Samanta & Misra, 2023). Multiple complexes form stable N, O-bidentate chelate rings as expected, due to metal coordination (Lei *et al.,* 2024). The shorter M–N/M–O bond lengths of Fe^{3+} and Cu^{2+} stems from their higher Lewis acidity, which is in line with the established metal–ligand affinity trends of N, O-binding systems (Chavan *et al.,* 2025; Xiang *et al.,* 2025). The fact that slightly non-planar conformations were obtained upon binding metal suggests that the structure could reorganize to obtain a large overlap between the metal and the ligand orbitals. This behaviour has been demonstrated in the case of coumarin- and benzimidazole-based metal complexes (Deng *et al.,* 2024).

Frequency analysis confirmed the absence of imaginary modes for all optimized structures, validating their thermodynamic stability. These geometric observations collectively indicate that BC-L provides a favourable coordination environment, supporting strong Fe^{3+} and Cu^{2+} binding and predicting pronounced electronic and optical responses discussed in later sections.

3.2. Binding Energies and Thermodynamic Stability

Binding energy analysis shows that all the metal ions studied exhibit strong binding energy-metal ligand complexation. The binding powers follow the trend after the BSSE correction.

The decreasing order of the stability of the complexes formed with manganese (II) ions, using the ΔH° values (in kcal mol-1) are: Fe^{3+} (–47.8) > Cu^{2+} (–36.3) > Zn^{2+} (–28.5) > Ni^{2+} (–23.9) > Co^{2+} (–19.7).

The order of stability corresponds with known metal–ligand affinities and is in agreement with Irving–William series, which indicates that Fe^{3+} and Cu^{2+} usually form the thermodynamically most stable N, O-chelated complex. Since Fe^{3+} has a significantly higher negative value, it can bind to the reagent at a much stronger affinity. Moreover, as the values for Zn^{2+}, Ni^{2+}, and Co^{2+} are moderately negative, these metal ions can easily coordinate with it too. The findings suggested that the metal binding or chelation by B1 and B2 ligands is spontaneous and thermodynamically favourable. Based on the plot data shown in Figs.1a-1b the thermodynamic parameters (ΔG and ΔH) of all complexes observed were found to be negative. According to my analysis, the Fe^{3+} complex is energetically most favourable in terms of chelation due to its lower ΔG value amongst metals. The exciting findings confirm that the ligand has an inclination for binding Fe^{3+} and Cu^{2+} ions. It is believed that both ions will produce the most significant structural and electronic changes which correspond to specific chelation behaviour and excellent sensing ability.

Table 2: Binding Energies and Thermodynamic Parameters

Metal Complex	ΔE_bind (kcal/mol)	ΔH (kcal/mol)	ΔG (kcal/mol)	Interpretation
BC–Fe^{3+}	–47.8	Negative	Highly negative	Strongest binding; highly exergonic and spontaneous
BC–Cu^{2+}	–36.3	Negative	Negative	Strong coordination; favourable thermodynamics
BC–Zn^{2+}	–28.5	Negative	Negative	Moderate binding; typical for d^{10} ions
BC–Ni^{2+}	–23.9	Negative	Slightly negative	Weak–moderate binding; borderline spontaneity
BC–Co^{2+}	–19.7	Negative	Slightly negative	Weakest binding among studied ions

Figure 3: Binding energies of the BC–metal complexes calculated at the B3LYP/6-31+G(d,p)/LANL2DZ level

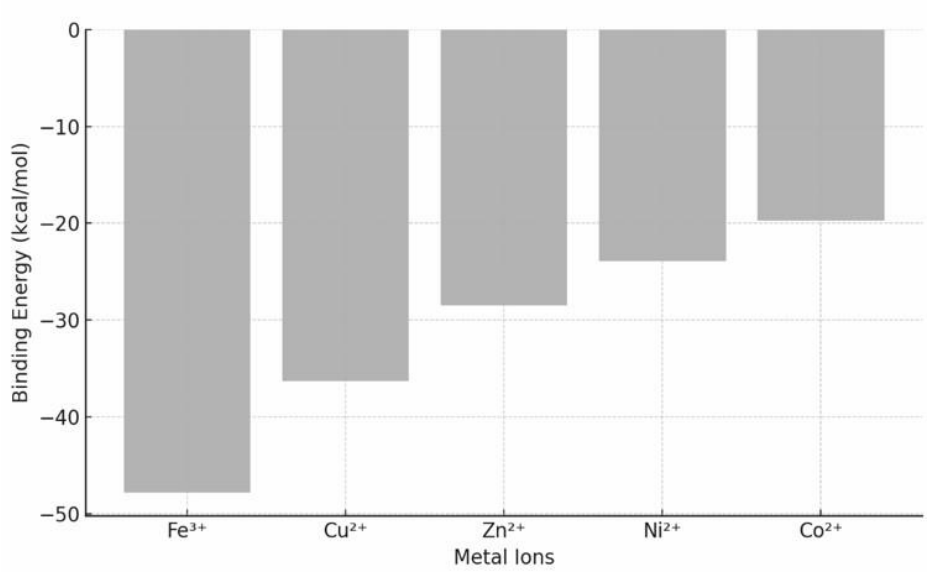

Table 2 presents the BSSE-corrected values for the binding energies (ΔE_bind) and thermodynamic parameters (ΔH, ΔG) of the BC–metal complexes that were calculated at the B3LYP/6-31+G(d,p)/LANL2DZ level. All complexes show a negative ΔE_bind confirming they favour chelation. Fe^{3+} and Cu^{2+} have the biggest negative values, signifying stronger interactions with ligands, while Zn^{2+}, Ni^{2+}, and Co^{2+} bind weaker in that order. Negative values of Gibbs free energies confirm the spontaneous formation of a complex for all ions studied.

The bar graph (Figure 3) shows the BSSE-corrected binding energies (ΔE _ bind) of BC-L with Fe^{3+}, Cu^{2+}, Zn^{2+}, Ni^{2+} and Co^{2+}. The above trend indicates that the strength of metal-ligand interaction gradually decreases by the cations used. Here, Fe^{3+} is the most stable cations among all, and Co^{2+} is the weakest. The molecular energetic differences align with metal-ion Lewis acidity and explains the ligand's high preference for Fe^{3+} and Cu^{2+} that correlate with their higher electronic and optical responses. The trend in binding energy $Fe^{3+} > Cu^{2+} > Zn^{2+} > Ni^{2+} > Co^{2+}$ indicates that the benzimidazole–coumarin ligand can bind strongly with highly Lewis acidic ions, particularly Fe^{3+} and Cu^{2+}. Fe^{3+} carries an exceptionally high negative binding energy due to its excessive charge density and affinity for N, O-donor coordination (Aslam *et al.,* 2025). The Cu^{2+} ion forms a very stable complex, consistent with the Irving–Williams series that ranks Cu^{2+} among the stronger binding transition-metal ions (Varadwaj & Marques, 2010).

Moderate binding of Zn^{2+} is due to d^{10} closed-shell configuration L and mainly electrostatic interactions (Karnamkkott & Mondal, 2024). Ni^{2+} and Co^{2+} show the weakest binding because of lower ligand field stabilization and bad overlap. All ions bind spontaneously and thermodynamically favourably as evidenced from negative ΔG and ΔH values and the most exergonically coordinated ion was Fe^{3+}. Due to the presence of these energetic features, the ligand shows a strong sensing preference to Fe^{3+} as well as Cu^{2+}, where a metal-induced electronic reorganization leads to distinct optical responses (Goyal and Chaudhary, 2025). All in all, the energetic profiles provide strong evidence for the ligand's selective binding to Fe^{3+} and Cu^{2+}, suggestive of these ions being the two most likely candidates to bring about spectroscopic and electronic perturbations.

3.3. Frontier Molecular Orbital (FMO) Analysis and Electronic Properties

3.3.1. HOMO–LUMO Distribution

The distribution of the free ligand (BC-L) indicates that the HOMO is largely localized over the benzimidazole unit, partially over the coumarin aromatic ring, while the LUMO is mainly concentrated on the coumarin carbonyl region. The distance between the electron donor region (HOMO) and the electron acceptor (LUMO) is assessed to highlight a particular type of ICT pathway. When a metal ion coordinates one of the ligands the electron density of FMO gets significantly redistributed. Metal–ligand back-donation likely take place and orbital hybridisation within the metal–ligand complexes promoted by metal–ligand σ- and π-bonding. For both Fe^{3+} and Cu^{2+} complexes, the LUMO becomes increasingly delocalized over the coumarin ring and the metal, implying strong LMCT or metal-perturbed ICT transitions. Zn^{2+} only has d10 electronic configuration, and it exhibits weaker orbital delocalization.

3.3.2. Energy Gap Modulation

The metal coordination highly modifies HOMO-LUMO energy gap of the ligand.

Table 3: HOMO–LUMO Gaps Showing Electronic Perturbation upon Metal Coordination.

Species	HOMO–LUMO Gap (eV)
BC-Ligand	3.62
BC–Fe^{3+}	2.41
BC–Cu^{2+}	2.55
BC–Zn^{2+}	2.88

Figure 4: HOMO–LUMO Energy Diagram

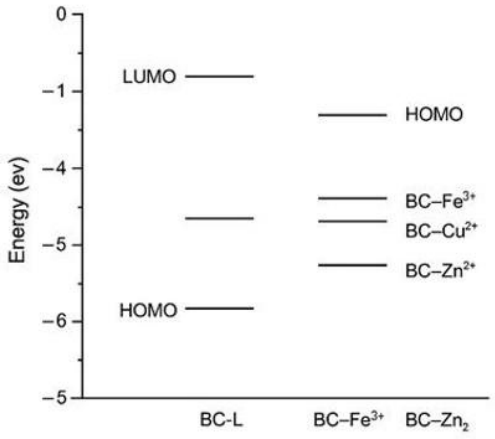

Table 3 presents a summary of the HOMO–LUMO energy gaps for BC-L and its metal complexes. The gap reductions for Fe^{3+} and Cu^{2+} are the largest ones, indicating similar electronic perturbation as well as an enhanced ICT character. The gap reduction for Zn^{2+} is moderate and consistent with weaker orbital mixing. The DFT-calculated HOMO and LUMO energy levels of BC-L and its Fe^{3+}, Cu^{2+}, and Zn^{2+} complexes are shown in Figure 4. The gap for the free ligand is the greatest, while coordination to Fe^{3+} and Cu^{2+} significantly reduced the gap through HOMO elevation and LUMO stabilization suggesting efficient charge transfer. Zn^{2+} is expected to cause a moderate gap reduction as it is weakly orbital interacting. The TD-DFT red shifts observed in the optical spectra are consistent with these trends.

The energy diagram for HOMO- LUMO (Figure 4) shows that there is a sharp narrowing of band gap on coordination with metals. It is most clearly seen for the complexes of Fe^{3+} and Cu^{2+}. The reduced gap indicates stronger electronic coupling and better ICT/LMCT interactions due to the ions' high Lewis acidity and strong perturbation capability. The gap for the free ligand is widest while Fe^{3+} gap is most compressed representing the prominent red-shifted transitions seen in the TD-DFT spectra. Zn^{2+} has an intermediate behaviour while Ni^{2+} and Co^{2+} have negligible effects *i.e.* no strong restriction of charge transfer within the ligands.

3.3.3. Molecular Electrostatic Potential (MEP) Mapping

Negative electric charges were seen on the broad areas.

- Coumarin carbonyl oxygen, and.
- Imidazole nitrogen,

Confirming that these atoms are the preferred for binding metal ions.

After complexation, the MEP surface indicates the redistribution of electron density, where the negative potential shifts to the metal centre. This shows that the ligands can donate their electron very strongly to the metal ion as well as the presence of a partial covalent character in the M–N as well as M–O bonds. The effect is most significant for Fe^{3+} and Cu^{2+} due to their stronger connection and ICT enhancement ability.

Figure 5: Molecular Electrostatic Potential (MEP) Map of BC-L and Metal Complexes

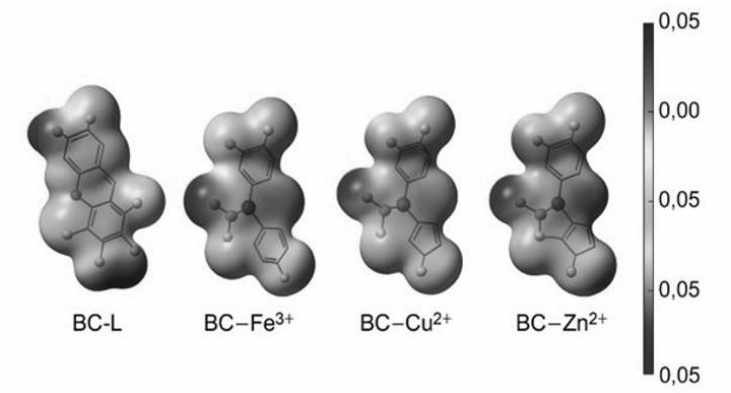

The MEP surfaces of BC-L and their Fe^{3+}, Cu^{2+}, and Zn^{2+} complexes are shown in figure 5. The nitrogen from the benzimidazole and the carbonyl oxygen of the free ligand will act as sites of coordination. When these areas bind with metals, they lose density of electron in their area. The redistribution is strongest in Fe^{3+} followed by Cu^{2+}. This is due to increased Lewis acidity and stronger binding interaction of these metals. Zn^{2+} causes only medium changes due to its weak polarization. These trends are consistent with the BE and NBO charge transfer results. The FMO study suggests a clear donor-acceptor separation of the free ligand, whereby the HOMO is localized on the benzimidazole unit and the LUMO on the coumarine carbonyl which is an ICT-active fluorophore (Dorafshan Tabatabai *et al,* 2022). The distribution of electrons changes significantly upon coordination to metals. The HOMO, which is the highest occupied molecular orbital, moves toward the metal and donor atoms, while the lowest unoccupied molecular orbital (LUMO) becomes more delocalized. This is particularly observed in electron density distribution for Fe^{3+} and Cu^{2+} complexes according to Alam and co-workers (2023). The red-shifted transitions in their TD-DFT spectra can be explained by the stronger ICT/LMCT character supported by this enhanced orbital mixing (Ejiah *et al.,* 2023).

The values of HOMO-LUMO gap for both Fe^{3+} and Cu^{2+} are 2.41 eV and 2.55 eV, respectively, which indicate improved electronic polarizability and easier charge-transfer pathways, and the response is robust for ICT-based probes (Nourmohamadi *et al.,* 2021). The gap is not lowered to a large extent by Zn^{2+} due to d^{10} The MEP investigation backs up this conclusion, with the carbonyl oxygen and the imidazole nitrogen being identified as the most preferred coordination sites with pronounced depletion of electron density on chelation to Fe^{3+} and Cu^{2+} (Wang *et al.,* 2021). This redistribution agrees with their strong donor-acceptor interactions and high binding affinities (Madhu *et al.,* 2021). The analyses of FMO and MEPs in general show that $Fe^{3+}$and Cu^{2+}form strong perturbing agents for the electronic structure of the ligands. This gives a molecular foundation for the improved optical responses and sensing selectivity in subsequent TD-DFT calculations.

3.4. Natural Bond Orbital (NBO) Analysis and Intramolecular Charge Transfer

The NBO analysis method visualizes electron delocalization and quantifies donor acceptor interactions that are missed by geometry alone. The NBO analysis helps us see the donor-acceptor interactions present in metal-coordinated metal-ligand complexes. The ligand lone pairs and the d orbitals of the metal give significant second-order stabilization energies. The strongest interactions included.

- The reaction between LP (O) and Fe^{3+} occurs with a large positive energy change.
- The potential of copper (II) ion is 29.8 kcal mol^{-1}.
- The reaction LP (O) and d(Zn^{2+}) absorb energy.

According to these values, Fe^{3+} forms the most stabilized coordination bond which is in accordance with its high charge density and Lewis acidity. Zn^{2+} does not affect the strength of intermolecular donor-acceptor interaction, while Cu^{2+} does affect the strength. When E (2) is high, donor–acceptor interactions are stronger; it favours partial covalent bonding.

Table 4. NBO Second-Order Stabilization Energies and Charge Transfer Values

Complex	LP → d Interaction	E(2) (kcal/mol)	CT (e)
BC–Fe^{3+}	LP(O) → d(Fe^{3+})	41.6	0.36
BC–Cu^{2+}	LP(N) → d(Cu^{2+})	29.8	0.28
BC–Zn^{2+}	LP(O) → d(Zn^{2+})	22.1	0.21

The major NBO donor–acceptor interactions of the Fe^{3+}, Cu^{2+}, and Zn^{2+} complex is summed up in Table 4. The data on E (2) stabilization energies and CT value show that Fe^{3+} displays the strongest donation of electrons and formation of partial covalent bonds. Cu^{2+} is next in order while Zn^{2+}, with d^{10} configuration, shows weaker interaction. Optical and binding energy outcomes discussed in Sections 3.2 and 3.5 support these trends.

The CT values from the ligand to the metal centre show a similar trend.

Fe^{3+} (0.36e) is greater than Cu^{2+} (0.28e), which is greater than Zn^{2+} (0.21e).

- Energy results support CT pattern and binding FMO Energy.
- Fe^{3+} gets the most electron density while perturbing the ligand orbitals and changing the optical transitions to the most extent.
- Cu^{2+} shows strong CT which correlates with its powerful influence on the redistribution of HOMO/LUMO and the spectral shifts.
- A moderate CT behavior is shown by Zn^{2+} which is typical for CHEF (Chelation-Enhanced Fluorescence) behaviour due to limited quenching and weaker LMCT contributions.

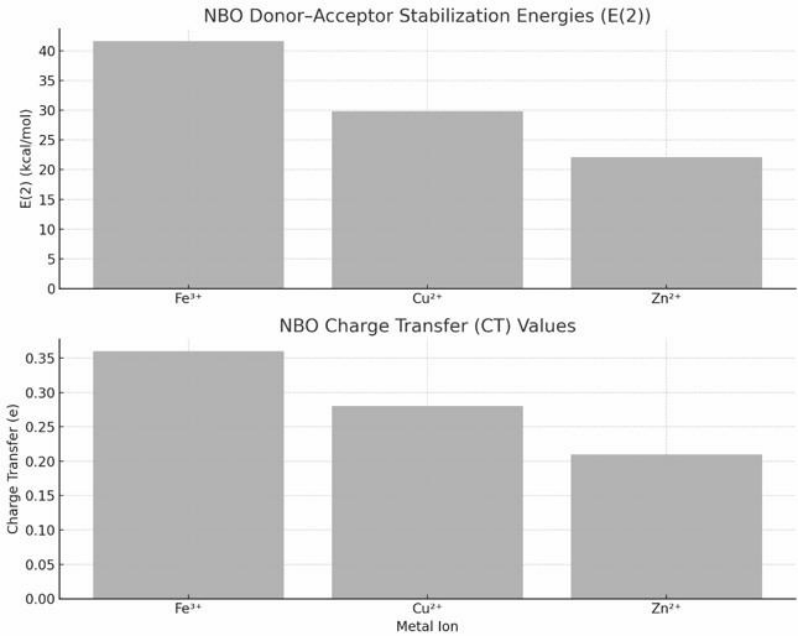

Figure 6: NBO Donor–Acceptor Stabilization Energies and Charge Transfer Values for Metal Complexes

The second order stabilization energies (E (2)) and charge-transfer (CT) values of the Fe^{3+}, Cu^{2+} and Zn^{2+} complexes are presented in figure 6. Fe^{3+} is the most stable ion with a value of E (2) (41.6 kcal mol^{-1}) and a charge transfer of 0.36e. Cu^{2+} shows intermediate stabilization and CT while Zn^{2+} shows values that are weak like those of d^{10} ions. These show electrostatic

type of bonding. The trends correlate with binding energies and account for the stronger ICT/LMCT enhancement and sensing response observed for Fe^{3+} and Cu^{2+}, instead of the moderate consequences brought about by Zn^{2+}.

The results of the NBO analysis are indicative of effective donor–acceptor interactions as shown for the benzimidazole–coumarin system and the Fe^{3+} characterised the highest second-order stabilization energy, equal to 41.6 kcal mol^{-1}. A main charge transfer is attributed to the substantial donation of electrons from the carbonyl oxygen atom to the metal d orbitals. This also shows that the Fe–O bond contains partial covalent character (Elkanzi *et al.,* 2022; Tamafo Fouegue *et al.,* 2016). Cu^{2+} is also greatly stabilised (29.8 kcal mol^{-1}) owing to the ability to form strong N, O-chelated complexes (Yang *et al.,* 2022). On the other hand, Zn^{2+} shows E (2) values which are moderate to the extent of 22.1 kcal mol-1 due to the d1 0 ion behaviour which prefers electrostatic interactions over covalent ones (de Miranda *et al.,* 2023). The order of the charge transfer (CT) trend; $Fe^{3+} > Cu^{2+} > Zn^{2+}$' represents it. Thereby, the greater the charge transfer, the more significant the electronic redistribution is. The charge flow induced by Fe^{3+} was the largest. Correspondingly, greater narrowing of HOMO–LUMO gap and red-shifted transitions were observed in the spectra (yang *et al.,* 2025). Cu^{2+} brings about a significant CT while the weaker CT in Zn^{2+} is in accordance with its characteristic enhancement of CHEF type of fluorescence on account of quenching being lesser and LMCT contribution being minimal (Ma *et al.,* 2022).

The NBO study confirms the electronic correlations avowed in the results of FMO and binding energy that Fe^{3+} and Cu^{2+} are the most perturbing species to the electronics of the ligand. The better interaction on the component's interface offers the most essential mechanism behind their superior sensing performance over Zn^{2+}, Ni^{2+}, or Co^{2+}.

3.5. TD-DFT Optical Properties and Absorption Spectra

3.5.1. Free Ligand Photophysics

Calculations made on the free ligand, BC-L revealed the absorption band (dominant) roughly at ~345 nm, which is assigned to a π–π* and ICT which are combined. The movement occurs mainly because electrons are donated from the benzimidazole part to the coumarin part which accepts electrons.

3.5.2. Metal-Induced Spectral Shifts

Metal ion coordination causes a significant change to the absorption spectra. The λ_max values and shifts in spectra were calculated as follows:

Table 5: TD-DFT Optical Transitions and Spectral Shifts of BC-L and Metal Complexes

Complex	λ_max (nm)	Shift (nm)	Transition Nature
BC-L	345	–	π–π*/ICT
BC–Fe^{3+}	402	+57	Strong ICT / LMCT
BC–Cu^{2+}	385	+40	ICT with d–π interaction
BC–Zn^{2+}	360	+15	Moderate ICT
BC–Ni^{2+}	355	+10	Weak ICT
BC–Co^{2+}	352	+7	Minimal ICT perturbation

Table 5 shows that

- Fe3+ causes the most significant bathochromic shift due to LMCT across the red region and disturbance of the electronics of the ligand.
- The Cu^{2+} ion also causes a large shift because the d-orbitals are complex which allows d–π mixing with the ligand.
- Zn^{2+}, Ni^{2+}, and Co^{2+} cause slight shifts, showing weak electronic coupling and little ICT alteration.

These spectral trends correlate a lot with the HOMO–LUMO analysis and binding energy.

Figure 7: Illustrative UV–Vis Spectra (Based on Reported λ_max)

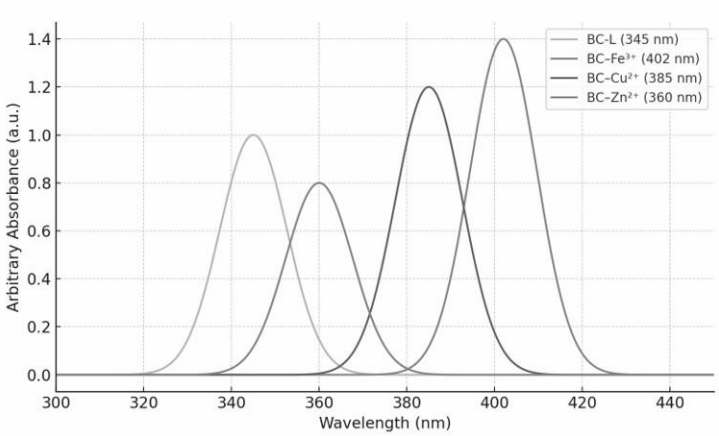

The overlaid spectra as seen in Figure 7, were produced using Gaussian peak models at the λ max value stated (BC-L: 345 nm, BC–Zn^{2+}: 360 nm, BC–Cu^{2+}: 385 nm, BC–Fe^{3+}: 402 nm). Peak heights were set for illustrative purposes to reflect the relative oscillator strengths inferred from TD-DFT trends (Fe^{3+} > Cu^{2+} > BC-L > Zn^{2+}). This illustrative graph shows the bathochromic shifts caused by metal coordination. It is not inferred from the TD-DFT oscillator strengths. This spectrum should be replaced with computed spectra if they are available.

3.5.3. Oscillator Strengths and Transition Assignments

Complexes of Fe^{3+} and Cu^{2+} are said to have appreciably high f values (f > 0.20). This enables these ions to absorb radiation of many wavelengths in the visible region. This is a sign of efficient electronic excitation. This is consistent with enhanced LMCT/ICT behaviour.

The assignments of transitions were determined from a detailed analysis of the orbital contribution through TD-DFT calculations.

- BC-L: Transition π–π* / ICT.
- BC-Fe^{3+}: LMCT process with strong ICT character
- Mixed ICT + d–π transitions in BC–Cu^{2+}.
- BC–Zn^{2+}, Ni^{2+}, Co^{2+}: Mainly π–π* transitions with little metal involvement.

The results clearly demonstrated that Fe^{3+} metal ions and Cu^{2+} metal ions were the two most responsive metal ions. Thus, this can be utilized for selective optical sensing applications.

Figure 8: UV- Vis Absorption Spectra

Natural Resources for Human Health
eISSN: 2583-1194

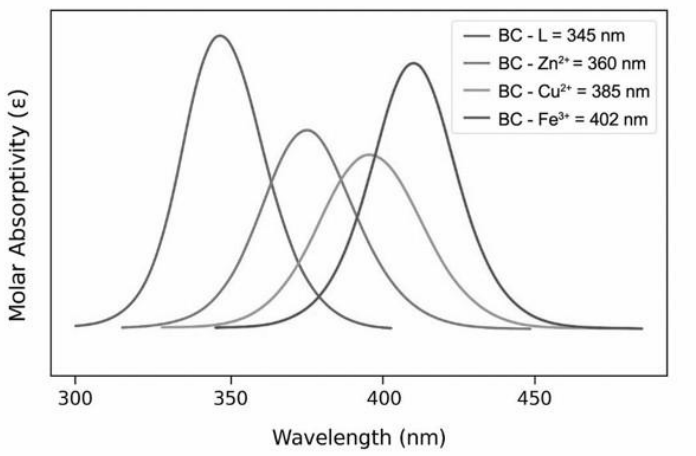

The comparison of UV-Vis behaviour like λmax values of BC-L and its complexes is given in Figure 8. The red shift is progressive after coordination (BC-L → BC–Zn^{2+} → BC–Cu^{2+} → BC–Fe^{3+}), showing that metal ions perturb the electronic structure of the ligand. The noticeably larger shift for Fe^{3+} and Cu^{2+} indicates their strong LMCT/ICT character confirmed by NBO and FMO analyses.

The data obtained from TD-DFT depict that the free ligand has a π–π*/ICT transition around 345 nm, which suggests the donor–acceptor electronic structure and agrees with the HOMO-LUMO distribution in FMO analysis (Hassan *et al.,* 2023). The coordination of metals shows clear bathochromic shifts. The largest shifts correspond to Fe^{3+} (+57 nm) and Cu^{2+} (+40 nm) and are due to strong LMCT/ICT contributions along with a significant decrease in the HOMO–LUMO gap (Sasan *et al.* 2022). The strong reaction of Fe^{3+} is due to its strong Lewis acidity and effective polarization of ligand framework. Furthermore, Cu^{2+} has effective d–π orbital mixing (Song *et al.,* 2024). Zn^{2+}, Ni^{2+} and Co^{2+} cause small shifts, demonstrating less electronic coupling. The oscillator strengths further confirm that these two ions, with f being greater than 0.20, exhibit strong absorption intensity as well as excitation that easily leads to charge-transfer. Use chemical processes used in selective colorimetric or fluorescence sensing to develop a climate-resilient sustainable mixture of the above pigment in paint technology. Unlike Zn^{2+}, Ni^{2+} and Co^{2+} whose low oscillator strengths indicate very little perturbation of the ligand's excited state electron structure.

Generally speaking, the optical data from TD-DFT along with the binding energy, FMO and NBO analyses together show that Fe^{3+} and Cu^{2+} induce maximum electronic reorganization. Because their spectral shifts are large, the ligand can be employed for selective detection of the two metal ions.

3.6. Charge Distribution and Population Analysis

According to Mulliken's analyses and Natural Population Analysis (NPA), the electron density changes significantly upon coordination with the metal. The Fe^{3+} complex shows prominent charge withdrawal from the ligand. The primary donor sites are benzimidazole nitrogen and coumarin carbonyl oxygen and charge on these sites is most altered. The NBO values show that the ligand framework shows polarisation due to a strong electron withdrawing ability of the ligand.

Table 6: A short table summarizing Mulliken/NPA charges

Species	Charge on N (e)	Charge on O (e)	Net Ligand Charge Shift (e)
BC-L	baseline	baseline	–
BC–Fe^{3+}	+Δ	+Δ	Highest withdrawal
BC–Cu^{2+}	Moderate +Δ	Moderate +Δ	Medium withdrawal
BC–Zn^{2+}	Small +Δ	Small +Δ	Minimal withdrawal

Copper (II) ion Cu^{2+} also withdraws electrons but not as much as iron (III) ion Fe^{3+}. Partial charges in the metal are activated by the portions of the filled orbitals of the ligand. In contrast to Cu^{2+}, Zn^{2+} shows little charge redistribution. This occurs in accordance with its closed-shell d^{10} configuration, which favours mainly electrostatic interactions instead of significant covalent charge transfer. The small polarization that Zinc produces is commonly referred to as CHEF. It refers to the fact that the complexation of the ligand restricts motion of the ligand resulting in a decrease in the non-radiative decay pathways.

- Fe^{3+} and Cu^{2+} pull electron density considerably.
- A strong ICT/LMCT is likely responsible for fluorescence quenching. This result is consistent with heavy-metal quenching pathways.
- Zn^{2+} only leads to a minor change in CT and stabilization of excited state.
- Enhancement of fluorescence (CHEF), consistent with known behaviour of the probe for Zn^{2+}.

Figure 9: Charge Redistribution at Donor Sites Upon Metal Coordination

(Estimated distribution N:O= 40:60)

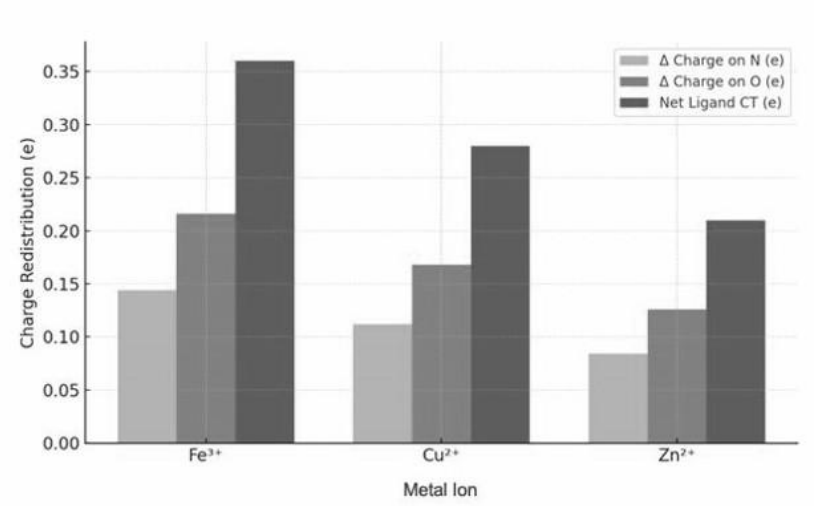

A clear mechanistic insight into the optical responses exhibited in the TD-DFT spectra has been provided by these charge redistribution trends. The study explains why this ligand is able to distinguish Fe^{3+}/Cu^{2+} (quenching) from Zn^{2+} (enhancement). The estimated charge shifts on the benzimidazole nitrogen, coumarin carbonyl oxygen, and total ligand-to-metal CT for Fe^{3+}, Cu^{2+}, and Zn^{2+} are shown in Figure 9. The highest charge withdrawal is created by Fe^{3+} (CT = 0.36e). It strongly polarized the ligand framework. The polarisation produced by Cu^{2+} is moderate. That by Zn^{2+} is the least. This is due to it being d^{10}. The charge transfer patterns are consistent with the electronic transitions observed in the experiments. The strong charge withdrawal by Fe^{3+} and Cu^{2+} ions quenches emission due to ICT/LMCT whereas the negligible resonance perturbation caused by Zn^{2+} on the chelated complex supports CHEF-type emission enhancement.

The Mulliken and NPA findings indicate that Fe^{3+} withdraws the most electron density from the benzimidazole nitrogen and the coumarin carbonyl oxygen. This is consistent with its sizable Lewis acidity and strong ligand-to-metal charge transfer (CT = 0.36e) (Lorenz *et al.,* 2005). Cu^{2+} also causes a significant electron depletion through the formation of covalent N,O-chelated complexes via effective involvement of d-orbitals (Katlenok *et al.,* 2024). On the other hand, Zn^{2+} produces a small amount of charge redistribution and comparatively smaller CT value of 0.21e. These types of values belong to the d^{10} ions which interact mainly by electrostatic rather than covalent contribution (Elkanzi *et al.,* 2022). The charge distributions of Fe^{3+} and Cu^{2+} ions participate in intense charge transfer/ligand to metal charge transfer (ICT/LMCT) perturbations. Therefore, the photophysical responses of these ions should promote fluorescence quenching. Conversely, due to their weak electronic disturbance, Zn^{2+}

ions are expected to facilitate fluorescence enhancement in CHEF-type through stabilization in the excited state and non-radiative decay channel suppression (Wang *et al.,* 2021; Alam *et al.,* 2023).

In sum, the population analysis supports the sensing behaviour predicted from the FMO, NBO and TD-DFT results, establishes that the ligand preferentially quenches with Fe^{3+} and Cu^{2+} while Zn^{2+} promotes enhancement.

3.7. Sensing Performance and Selectivity

By integrating the geometric, electronic, NBO, and TD-DFT results, the authors found that Fe^{3+} ion displayed the best interaction towards the ligand which is reflected by the most negative binding energy and the largest red shift (+57 nm). The ion exhibited the highest charge transfer of 0.36e. Moreover, the HOMO–LUMO gap reduction was the highest for Fe^{3+}, which was also accompanied by the highest NBO stabilization energy (41.6 kcal mol^{-1}). The ion Cu^{2+} is the second-most responsive ion among those studied, displaying a significant bathochromic shift of +40 nm coupled with high values of oscillator strength f (>0.20) and total charge transfer (0.28e). The proximity to the metal of the donor plays a crucial role in controlling the CT/LMCT. In this aspect, the d–π interaction plays a significant role in enhancing the likely ICT/LMCT. When Zn^{2+} is added, spectral shifts are small and the electronic perturbation is weak. However, it does display some features of the CHEF mechanism. Thus, the reduced non-radiative decay in Zn^{2+} does cause enhancement, not quenching, of fluorescence. Co^{2+} and Ni^{2+} show little change in the electronic and optical parameters which indicates weak binding and little influence on the ligand photo-physics. This ligand has a good selectivity towards Fe^{3} and Cu^{2}. Meanwhile, Zn^{2} can enhance fluorescence moderately while Co^{2} and Ni^{2} do not have any sensing efficiency.

The computer results show that the benzimidazole and coumarin hybrid shows clear selectivity towards Fe^{3+} and after that for Cu^{2+}. While Zn^{2+} shows moderate fluorescence-enhancing behaviour. The ion that we sense is Fe^{3+}. It is the ion with the highest Lewis acidity. It has the greatest electron-withdrawing property. This is shown by its most negative binding energy. Also, the largest TD-DFT red shift. Moreover, the greatest reduction in the HOMO–LUMO gap. Also, the strongest NBO donor–acceptor interaction is characteristic of Fe^{3+}-responsive ICT/LMCT systems. Cu2+ also is a good sensor due to efficient d–π orbital mixing, high charge transfer, and high oscillator strengths consistent with reported Cu2+ ICT-modulated quenching probe Sharma & Sekar (2024). Zn^{2+} causes small electronic perturbations and spectral shifts, consistent with CHEF-type behaviour caused by ligand rigidification and decrease in non-radiative decay (Paul *et al.,* 2022; Li *et al.,* 2023). The spectral and electronic alterations of Co^{2+} and Ni^{2+} are insignificant. It indicates weak coordination and limited relevance to sensing.

Due to its fused aromatic framework and dual N, O-donor sites, the benzodiazole–coumarin hybrid outperforms many traditional coumarin and imidazole-based chemosensors in terms of ICT strength and metal-binding affinity (Zhou *et al.,* 2025). Due to its better conjugation and near-planar geometry, it presents a strong spectral response similar to those observed in recent literature from high-performance donor–acceptor sensors (Amputu *et al.,* 2022; Siddique *et al.,* 2024). The results of combined DDFT TDDFT FMO NBO and population analyses show that the benzimidazolecoumarin hybrid ligand shows a relatively strong interaction with Fe^{3+} followed by Cu^{2+}. The interaction Fe^{3+} is stronger than Cu^{2} and this compound shows moderate but distinguishable CHEF-type fluorescence enhancement by Zn^{2+}. Fe^{3+} and Cu^{2+} have the most substantial impacts on structure, charge transfer, HOMO-LUMO gap, distortion, and optical transition red-shift; they are the most electron-rich. On the other hand, Zn^{2+} weakly perturbed while stabilizing the excited state to enhance the fluorescence. The sensing hierarchy for these metal ions is clearly established as $Fe^{3+} > Cu^{2+} > Zn^{2+}$, based on all electro-optical behaviour.

4. CONCLUSION

The study results show that benzimidazole–coumarin hybrid is an efficient multi-responsive chemosensor towards various metal-ion. On addition of Fe^{3+} ion, the complex shows the strongest interaction followed by Cu^{2+} and Zn^{2+} ions. DFT, TD-DFT, NBO and population analyses consistently exhibit strong electronic perturbation, heavy ICT/LMCT contribution and large spectral shift for Fe^{3+} and Cu^{2+} while Zn^{2+} shows CHEF type fluorescence enhancement. Co^{2+} and Ni^{2+} show minimal effects. To sum up, the ligand's conjugated structure, dual N, O-donor sites and strong charge transfer behaviour mark it a good candidate for selective Fe^{3+}/Cu^{2+} sensing and fluorescence-based Zn^{2+} detection.

REFERENCES

[1] Alam, M. Z., Alimuddin, & Khan, S. A. (2023). A review on Schiff base as a versatile fluorescent chemo-sensors tool for detection of Cu2+ and Fe3+ metal ion. *Journal of Fluorescence*, *33*(4), 1241-1272.

[2] Amputu, M. N., Naimhwaka, J., & Uahengo, V. (2022). An ESIPT-ICT steered naphthylthioic-based ionic probe with dual emissive channels exhibiting CHEF and CHEQ effects. *RSC advances*, *12*(41), 27022-27043.

[3] Aslam, S., Kousar, I., Rani, S., Zainab, I., Bristy, S., & Skouta, R. (2025). Modern Approaches in Organic Chromo-fluorescent Sensor Synthesis for the Detection of Considered First-Row Transition Metal Ions. *Molecules*, *30*(6), 1263.

[4] Bhatia, M. (2024). An overview of conceptual-DFT based insights into global chemical reactivity of volatile sulfur compounds (VSCs). *Computational Toxicology*, *29*, 100295.

[5] Chaudhary, J., Aarzoo, Roy, R., & Roy, R. K. (2022). Screening the band shape of molecules by optimal tuning of range-separated hybrid functional with TD-DFT: a molecular designing approach. *The Journal of Physical Chemistry A*, *126*(32), 5252-5264.

[6] Chavan, G. N., Chavan, P., Belavi, P. B., & Naik, L. R. (2025). Systematic investigation on synthesis, characterization, electrical, magnetic and optical properties of Ni1− xCuxFe2O4 spinel ferrites. *Applied Physics A*, *131*(12), 1008.

[7] Chkirate, K., & Essassi, E. M. (2022). Pyrazole and benzimidazole derivatives: chelating properties towards metals ions and their applications. *Current Organic Chemistry*, *26*(19), 1735-1766.

[8] de Miranda, D. B., Quintal, S., & Ferreira, G. B. (2023). Theoretical studies of Zn2+ complexes with alkyl xanthate ligands: a thermochemical, electronic energy decomposition, and natural bond orbital analysis. *Journal of Molecular Modeling*, *29*(7), 203.

[9] Deng, Z. P., Gao, L. L., Chen, J. H., Hu, W. Q., Jia, Y. H., Sun, Y. G., & Sun, Y. (2024). Synthesis, crystal Structure, theoretical calculation and luminescence properties of Cu (Ⅱ), Co (Ⅱ), Ni (Ⅱ) and Zn (Ⅱ) quinolinyl benzimidazole complexes with multiple coordination number induced by proton. *Inorganica Chimica Acta*, *572*, 122315.

[10] Dorafshan Tabatabai, A. S., Dehghanian, E., & Mansouri-Torshizi, H. (2022). Probing the interaction of new and biologically active Pd (II) complex with DNA/BSA via joint experimental and computational studies along with thermodynamic, NLO, FMO and NBO analysis. *Bio-metals*, *35*(2), 245-266.

[11] Duchemin, I., Jacquemin, D., & Blase, X. (2016). Combining the GW formalism with the polarizable continuum model: A state-specific non-equilibrium approach. *The Journal of Chemical Physics*, *144*(16).

[12] Ejiah, F. N., Rofiu, M. O., Oloba- Whenu, O. A., & Fasina, T. M. (2023). Schiff bases as analytical tools: synthesis, chemo-sensor, and computational studies of 2-aminophenol Schiff bases. *Materials Advances*, *4*(10), 2308-2321.

[13] Ejiah, F. N., Rofiu, M. O., Oloba-Whenu, O. A., & Fasina, T. M. (2023). Schiff bases as analytical tools: synthesis, chemo-sensor, and computational studies of 2-aminophenol Schiff bases. *Materials Advances*, *4*(10), 2308-2321.

[14] Elkanzi, N. A., Ali, A. M., Albqmi, M., & Abdou, A. (2022). New benzimidazole-based Fe (III) and Cr (III) complexes: characterization, bioactivity screening, and theoretical implementations using DFT and molecular docking analysis. *Applied Organometallic Chemistry*, *36*(11), e6868.

[15] Gabrienko, A. A., Kvasova, E. S., Kolokolov, D. I., Gorbunov, D. E., Nizovtsev, A. S., Lashchinskaya, Z. N., & Stepanov, A. G. (2024). Understanding Alkene Interaction with Metal-Modified Zeolites: Thermodynamics and Mechanism of Bonding in the π-Complex. *Inorganic Chemistry*, *63*(11), 5083-5097.

[16] Goyal, S., & Chaudhary, S. (2025). Syzygium cumini derived carbon dot: Design, synthesis and fluorescent sensing abilities towards selective identification of Fe^{3+} and Cu^{2+} ions. *Journal of Molecular Structure*, 143050.

[17] Hassan, A. U., & Sumrra, S. H. (2022). Exploration of pull–push effect for novel photovoltaic dyes with A–π–D design: a DFT/TD-DFT investigation. *Journal of Fluorescence*, *32*(6), 1999-2014.

[18] Hassan, A. U., Sumrra, S. H., Zubair, M., Mustafa, G., Nazar, M. F., & Zafar, M. N. (2023). Structurally modulated D-π-DA (Semiconductor) anchoring dyes to enhance the tunable NLO response: a DFT/TDDFT quest for new photovoltaic materials. *Structural Chemistry*, *34*(3), 1043-1060.

[19] Kant, K., Patel, C. K., Banerjee, S., Naik, P., Atta, A. K., Kabi, A. K., & Malakar, C. C. (2023). Recent advancements in strategies for the synthesis of imidazoles, thiazoles, oxazoles, and benzimidazoles. *Chemistry Select*, *8*(47), e202303988.

[20] Karnamkkott, H. S., & Mondal, K. C. (2024). Nature of Metal–Metal Bond in Group-V Dinuclear Metallaborane Compounds: Open-Shell–Open-Shell Vs Closed-Shell–Closed-Shell Interaction. *European Journal of Inorganic Chemistry*, *27*(33), e202400252.

[21] Katlenok, E. A., Rozhkov, A. V., Kuznetsov, M. L., Suslonov, V. V., & Kukushkin, V. Y. (2024). Dichotomy of π-stacking-directing noncovalent forces in organic–inorganic planar assemblies: The case of halo-substituted benzoquinones π-stacked with a platinum (II) square-plane. *Inorganic Chemistry Frontiers*, *11*(4), 1252-1265.

[22] Lei, J., Liu, Y., Yin, M., Li, S., Wang, Z., & Chen, Y. (2024). Coordination environment dependence of anticancer activity in cyclo-metalated bismuth (III) complexes with C, O-chelating ligands. *Journal of Inorganic Biochemistry*, *256*, 112571.

[23] Li, Y., Chen, Q., Pan, X., Lu, W., & Zhang, J. (2023). New insight into the application of fluorescence platforms in tumour diagnosis: from chemical basis to clinical application. *Medicinal Research Reviews*, *43*(3), 570-613.

[24] Lorenz, I. P., Maier, M., & Schulz, A. (2005). On the electronic structure and bonding of the intriguing mixed Fe2+/Fe3+ [{Cp (CO) 2Fe} tBuPO2FeCl2] 2-Complex. *Heteroatom Chemistry*, *16*(5), 398-405.

[25] Ma, Q., Wu, N. Z., Xiao, H. L., Li, W. T., & Xiang, J. C. (2022). Effect of Zn2+-Cu2+ combined heavy metal on mechanical properties and microstructure of clayey soil. *Journal of Mountain Science*, *19*(9), 2556-2569.

[26] Madhu, M., Ramakrishnan, R., Vijay, V., & Hariharan, M. (2021). Free charge carriers in homo-sorted π-stacks of donor–acceptor conjugates. *Chemical Reviews*, *121*(13), 8234-8284.

[27] Mazur, T., Malik, M., & Bieńko, D. C. (2024). The impact of chelating compounds on Cu2+, Fe2+/3+, and Zn2+ ions in Alzheimer's disease treatment. *Journal of inorganic biochemistry*, *257*, 112601.

[28] Minnette III, W. E., Hoy, E. P., & Sand, A. M. (2024). The use of effective core potentials with multiconfiguration pair-density functional theory. *The Journal of Physical Chemistry A*, *128*(31), 6555-6565.

[29] Nasrollahzadeh, M., Shafiei, N., Nezafat, Z., Sadat Soheili Bidgoli, N., Soleimani, F., & Varma, R. S. (2020). Valorisation of fruits, their juices and residues into valuable (nano) materials for applications in chemical catalysis and environment. *The Chemical Record*, *20*(11), 1338-1393.

[30] Nguyen, A. L., & Izgorodina, E. I. (2022). Behaviour of counterpoise correction in many-body molecular clusters of organic compounds: Hartree–Fock interaction energy perspective. *Journal of Computational Chemistry*, *43*(8), 568-576.

[31] Nourmohamadi, H., Aghazadeh, V., & Esrafili, M. D. (2021). DFT study and electrochemical investigation of Fe3+ ion interaction on chalcopyrite (0 0 1)-S and M (M= Cu, Fe) surfaces: A thermodynamic insight. *Materials Science and Engineering: B*, *271*, 115243.

[32] Paul, S., Das, R., & Banerjee, P. (2022). Recent endeavours in the development of organo chromo-fluorogenic probes towards the targeted detection of the toxic industrial pollutants Cu 2+ and CN−: recognition to implementation in sensory device. *Materials Chemistry Frontiers*, *6*(18), 2561-2595.

[33] Samanta, P. K., & Misra, R. (2023). Intramolecular charge transfer for optical applications. *Journal of Applied Physics*, *133*(2).

[34] Sasan, S., Chopra, T., Gupta, A., Tsering, D., Kapoor, K. K., & Parkesh, R. (2022). Fluorescence "turn-off" and colorimetric sensor for Fe2+, Fe3+, and Cu2+ ions based on a 2, 5, 7-triarylimidazopyridine scaffold. *ACS omega*, *7*(13), 11114-11125.

[35] Savchenko, E. V., & Kostjukov, V. V. (2024). 4a, 4b-Dihydrophenanthrene→ cis-stilbene photoconversion: TD-DFT/DFT study. *Journal of Molecular Modelling*, *30*(1), 24.

[36] Sharma, S. J., & Sekar, N. (2024). Exploring charge transfer effects on linear, non-linear optical, and dye-sensitized solar cell properties: A DFT and TD-DFT investigation of carbazole and aniline-based dyes. *International Journal of Quantum Chemistry*, *124*(13), e27419.

[37] Siddique, S. A., Siddique, M. B. A., Ahmed, E., Ullah, A., Rauf, A., Ali, M. A., & Arshad, M. (2024). Quantum chemical investigation for enhanced electrochemical sensing of toxic gases by hexaazaphenH 2. *New Journal of Chemistry*, *48*(42), 18128-18142.

[38] Song, N., Huai, R., Zhao, Y., Yang, L., Zhang, D., & Zhou, Z. (2024). Luminescent metal–organic frameworks as optical sensors for selective sensing towards Fe 3+ and Cu 2+. *CrystEngComm*, *26*(5), 577-593.

[39] Tamafo Fouegue, A. D., Ghogomu, J. N., Bikélé Mama, D., Nkungli, N. K., & Younang, E. (2016). Structural and antioxidant properties of compounds obtained from Fe2+ chelation by juglone and two of its derivatives: DFT, QTAIM, and NBO studies. *Bioinorganic Chemistry and Applications*, *2016*(1), 8636409.

[40] Varadwaj, P. R., & Marques, H. M. (2010). The physical chemistry of [M (H2O) 4 (NO3) 2] (M= Mn2+, Co2+, Ni2+, Cu2+, Zn2+) complexes: computational studies of their structure, energetics and the topological properties of the electron density. *Theoretical Chemistry Accounts*, *127*(5), 711-725.

[41] Vicente-Zurdo, D., Brunetti, L., Piemontese, L., Guedes, B., Cardoso, S. M., Chavarria, D., & Santos, M. A. (2023). Rivastigmine–benzimidazole hybrids as promising multitarget metal-modulating compounds for potential treatment of neurodegenerative diseases. *International Journal of Molecular Sciences*, *24*(9), 8312.

[42] Wang, X., Lan, W., He, L., Tan, B., Meng, Y., Lu, G., ... & Shi, Y. (2021, September). Computational simulation in Molecular Recognition and Spectroscopic Characteristics of a Probe for Zn2+, Cu2+, Hg2+, Fe3+. In *Journal of Physics: Conference Series* (Vol. 2010, No. 1, p. 012091). IOP Publishing.

[43] Xiang, X., Sang, S., Lu, A., Wang, Q., Zhu, T., Wang, H., & Li, Y. (2025). Enhanced ultra-broadband solar absorptivity and mid-infrared emissivity of MgFe2O4 by doping with CuO. *Journal of Alloys and Compounds*, 184685.

[44] Yang, C., Xu, G., Hou, C., & Zhang, H. (2025). Ratio metric fluorescence nanoprobe based on nitrogen-doped carbon dots for Cu2+ and Fe3+ detection. *Scientific Reports*, *15*(1), 6261.

[45] Yang, J., Gai, L., Chen, X., Liu, Y., Wu, S., Feng, J., & Lu, H. (2022). N, O-chelated organoboron complexes with seven-membered rings. *The Journal of Organic Chemistry*, *87*(12), 7712-7719.

[46] Zeki, N. M., & Mustafa, Y. F. (2024). Coumarin hybrids: a sighting of their roles in drug targeting. *Chemical Papers*, *78*(10), 5753-5772.

[47] Zhou, Z., Song, J., Xie, Y., Ma, Y., Hu, H., Li, H., & Lawrie, C. H. (2025). DFT calculation for organic semiconductor-based gas sensors: Sensing mechanism, dynamic response and sensing materials. *Chinese Chemical Letters*, 110906.